Study of critical failure surface influencing factors for loose rock slope

Shuhong Wang[1] · Zulkifl Ahmed[1] · Pengyu Wang[1]

Abstract

In current research, a novel geometrical technique is introduced to estimate the length (L) of sliding arc by considering slip surface entry point distance (d_e). Morgenstern-Price limiting equilibrium and strength reduction methods are selected within the framework of SLOPE/W and FLAC^{3D} softwares respectively, to study the sliding mechanism and stability-effecting factor for a loose rock slope comprise of two different material. Also, the variability influence of strength parameters (cohesion force and friction angle) and the depth of pore water pressure on safety factor, failure depth (D) and distribution range of critical failure surface (CFS) are investigated through software. The results show that the shear strength parameters and the depth of pore water pressure plays a significant role in altering overall stability and the distribution range of CFS for a loose rock slope. Shallow failure with composite failure surface is much easier to occur for loose rock slope subjected to pore water pressure and material heterogeneity. These findings can be effectively used for loose rock slope reinforcement design.

1 Introduction

Engineers mostly investigate rock slope stability to precisely classify the most distinct 2D/3D possible critical slip surface [1]. Engineers also use several analytical methods to evaluate the stability factor of natural or artificial slopes [2]. Limit equilibrium techniques are leading among these methods, in which the empirically based established site-stability charts may be applicable for slope stability calculation in certain conditions [3]. In general, nevertheless, laboratory tests, field assessment and more precise numerical solutions are normally suggested [4]. The outcomes of above studies are usually reported as the probability of failure and FS for the geotechnical parameters [4].

Although the limiting equilibrium (LE) method extensively used for stability analysis, is lacking in definite respects: predominantly, the incapability of the technique to consider the multifaceted constitutive relations of the slope materials [5, 6]. Furthermore, during LE calculations assumptions are made by which water influences are isolated, because the influences of preliminary stresses are not straightforwardly incorporated, and this is impossible to compute local safety factors for slope [7, 8]. So, the position of the CFS is found capably and comparatively easily if the resultant explanation of the slope is adequate with the range of the available geotechnical data.

Limit-equilibrium approaches are also widely selected for slope stability investigation, mainly due to their ease of use and simplicity. Among these techniques, the technique of slices selected with a circular sliding surface (CSS) and frequently employed when the circles are often approximate and convenient to analyse the studied failure surface [2]. Inappropriately, there are several cases, in which simple slip-circle technique cannot be applied for stability analysis and any choice of the nature of the failure surface cannot be commonly useable for further study. This is particularly

---

✉ Zulkifl Ahmed, ahmdani688@gmail.com | [1]School of Resource and Civil Engineering, Northeastern University, Shenyang 110819, China.

due to the heterogeneous profiles of slope wherein a critical sliding surface (CSS) is anticipated to make parallel with the line of minimal resistance for example anisotropy, bedding, etc. In the site, examinations of actual sliding surfaces show that circular failure surfaces can indicate the variety of characters with severe changes at the boundary between dissimilar geological materials [9, 10]. Hence, circular failure surface can referred to the distinct case of noncircular sliding exploration where the previous is considered a systematic method. Therefore, the conventional limit equilibrium study for the slope stability factor assessment includes two phases: (a) development of a law of resemblance in between the safety factor and a probable sliding surface. (b) Searching for the minimum value of safety factor (FS) and over all realistic sliding surface, which shows minimum value of FS, is refer to critical sliding surface (CSS).

Significant effort already has been made to the first aspect; the techniques of Bishop [11], Baker [12], extended Spencer [13], and a global procedure of Morgenstern and Price [14] are well known today. In the second aspect, various techniques have been used to analyze the location of the critical sliding surfaces [15, 16]. These methods are not particularly laborious [17]. But, numerical methods are useful for slope stability assessment [18], and key block analytical method can be used for rock slope failure analysis [19]. Blocky structural sliding of rock slope is analyzed by using fuzzy key-block method [20]. Simple genetic algorithm [21] and ant colony optimization [22] are applicable for critical non-circular failure surface of rock slope stability analysis. A suitable method of stability calculation can be determined by a combination of the above logical methods. The position and size of the critical failure surface cannot be determined well with limit-equilibrium techniques. But, nural network and optimization algorithm could be easily selected to define its position [23, 24].

In current research, a simple geometrical scheme is introduced first time to calculate the failure arc (L) of a loose rock slope. SLOPE/W computer code is used to analyze the failure mechanism of CFS of a real case of instability. In addition, the effect of cohesion, internal friction and pore water pressure on the distribution of CFS is studied by software. At last, FLAC[3D] software is also selected to check the correctness of results evaluated from SLOPE/W. In these findings, the CFS allocation will provide concrete guidelines for choosing the more typical sliding surface in risk assessments and system reliability analyses of heterogeneous loose rock slope beside road.

2 Methodology

There are numerous approaches selected for slope stability investigation. Among these approaches, the limiting equilibrium (LE) technique of slices [25–27] have attracted significant attention, due to its accuracy and simplicity. In this process, the ratio between the resisting forces to driving forces on a possible slip surface is well-defined as the probability of slid. Only if the intended value of FS more than one then slope is thought-out safe. Limiting equilibrium calculations consider the slope failure surface as a rigid body [28]. Sliding body or surface delivers necessary information and has been extensively adopted previously to evaluate the stability of all types of slopes. For example the stability of heterogeneous slopes was calculated with the help CFS to take safety measures [27], for dam slopes [29], rock slopes [30], highway slopes [31] and rock cliff face [32].

The limiting equilibrium procedures are frequently used as the systematic approaches to determine the stability of weathered rockslides. In geotechnical engineering field, investigating the stability of slopes are also one of the oldest kinds of study. In the 20th century many researcher presented the knowledge of dividing the probable sliding mass into several number of slices for stability determination purpose [27, 33]. In the 1960's due to the dawn of computers technology, which made it conceivable to extra voluntarily switch for iterative measures which are essential scheme to control the statistically more laborious equations [33]. On the other hand, the idea of numerically discretizing a large slippery mass into small parts for investigation objectives is relatively innovative at the time. Moreover, in LE calculations assumptions are made first to generalize the effects of water pressure and comprehensively incorporate the influence of primary stresses. In addition, this is impossible to evaluate potential FS. However, if the resultant generalization of the problem is appropriate or acceptable with the scope of the existing geotechnical information than the position of the CSS could be found quite efficiently easily.

SLOPE/W computer program is a product of Geo-Studio software system. One of the more commanding topographies of this joined tool is that this provides access to sorts of investigates of a complex and broader field of difficulties, together with the selection of stresses and calculated water pressures in the stability study. It is possible in limit equilibrium (LE) computer programs such as SLOPE/W to deal with extremely irregular water pressure, complex stratigraphy, variety of nonlinear and linear strength models, material heterogeneity, concentrated loads, structural reinforcement and practically any

type of sliding surface shape [34]. Then search method is prolonged to compare the CSS for a loose slope.

2.1 Determination of shear strength parameters

To estimate the unknown material constants, such as cohesion (*c*) and internal friction angle (ϕ), a new C-tanφ relationship chart is first created from multiple sliding surfaces within the framework of SLOPE/W tool as shown in Fig. 1. Two curves showing the C/ϕ relationships can be plotted by using the method of slice [35]. Set the hypothetical safety factor of the said slope intended for repeated calculation to be one. The following lists of strata whose soil constants are; sandy soil: unit weight $\gamma_t = 18.0$ (kN/m^3), friction angle ϕ (°) and cohesion force *c* (kN/m^2) were determined from reverse calculation by using density of water γ_w is 9.80 (kN/m^3). Weathered rock: unit weight $\gamma_t = 20.0$ (kN/m^3), friction angle ϕ = 34° and cohesion *c* = 15 (kN/m^2). The unknown constants (*c* and ϕ) for sandy soil were then determined from C-tanϕ relational expression diagram (Fig. 1), by assuming that 120 m^2 area of slope have *c* = 1 KN/m^2. With reference to the Fig. 1, the value of *c* and tanϕ is noted *c* = 15.3 KN/m^2 and tanϕ = 0.41 (ϕ = 25°).

2.2 General limit equilibrium formulation

Figure 2 shows a representative failure surface (*AB*), failure arc (*L*), slices discretization scheme and the forces acting on a slice of the slope. Normal forces (*E*) and shear forces (*X*) are acting on the base and one sides of the slice, respectively (Fig. 2). Limit equilibrium (LE) calculation is consist on two safety factors calculations and permits for a boundary of inter-slice normal-shear force circumstances. One calculation gives the FS regarding
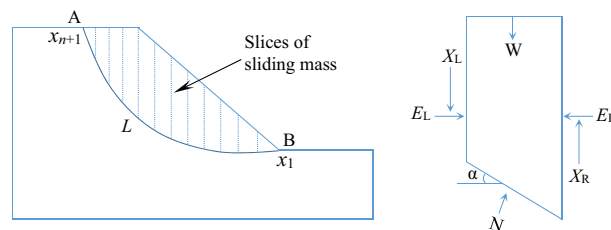

Fig. 2 Slice discretization and forces acting on a slice

horizontal force (F_f) while the other calculation provides the FS with regard to moment (F_m). An equation to handle inter-slice shear forces can be written as:

$$X = E\lambda f(x) \qquad (1)$$

where *X* = shear force, *E* = normal force, λ = dimensionless function and *f(x)* = a function. In current analysis, a distinctive half-sine function is chosen in SLOPE/W software as shown in Fig. 3. In this figure, the upper and lower curves are actual specified and used functions. Lambda (λ) is the ratio between the two curves. One of the basic problems in LE calculation is knowing how to describe interslice and FS equation relating to moment equilibrium is:

$$F_m = \frac{\sum(c'\beta R + (N - u\beta)R\,tan\phi')}{\sum wx - \sum N_f \pm \sum D_d}. \qquad (2)$$

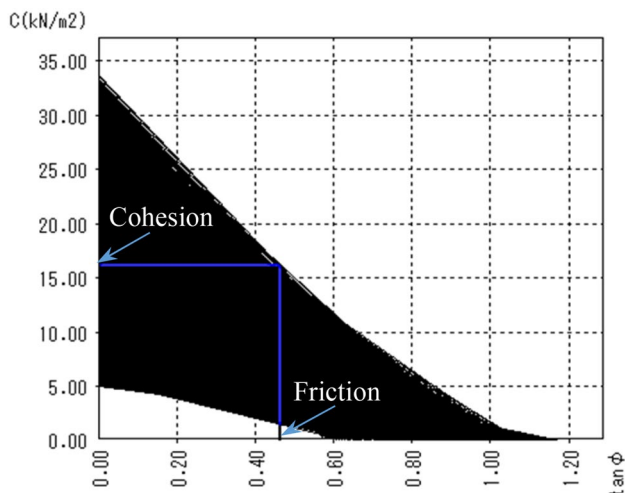The safety factor (FS) equation regarding horizontal force equilibrium is:
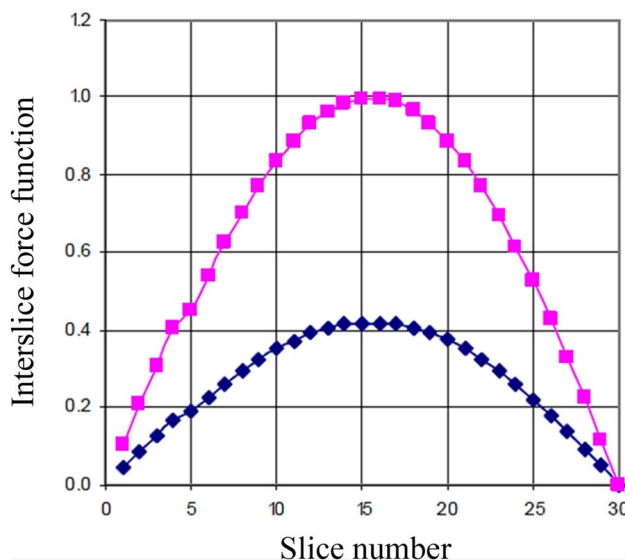

Fig. 1 C-tanϕ relationship diagram

Fig. 3 Half-sine interslice force function

$$F_f = \frac{\sum(c'\beta\,cos\alpha + (N - u\beta)tan\phi'cos\alpha)}{\sum N\sin\alpha - \sum D cos\omega}. \tag{3}$$

Base normal is defined as:

$$N = \frac{W + (X_R - X_L) - \frac{(c'\beta\,sin\alpha + u\beta\,sin\alpha\,tan\phi')}{F}}{cos\alpha + \frac{sin\,\alpha\,tan\phi'}{F}}. \tag{4}$$

In above equations, ϕ' = effective internal angle of friction, c' = effective cohesion, N = base normal force, u = water pressure, W = slice weight, α = slice base inclination, D = point load and β, x, R, f, ω, d are geometric parameters.

Equation 4 is acquired by the summation of all vertical forces. $F = Fm$, when base normal force N is substituted in the Eq. 2 and $F = F_f$ when N is substituted in Eq. 3. The normal force (N) is dependent on the inter-slice shear forces (X_R and X_L) on both sides of the slice.

Limit equalibrium formulation calculates F_f and F_m a choice of dimensionless function (λ) values. A plot is shown in Fig. 4, which was computed to illustrate how F_f and F_m vary with lambda (λ). At the end, for the whole slope there is only one FS. F_f and F_m are similar when both force and moment equilibrium were satisfied and FS was same for each slice.

2.3 Determination of failure arc

A new geometrical procedure is developed to calculate L. Figure 5 shows a possible geometry of a failure surface with
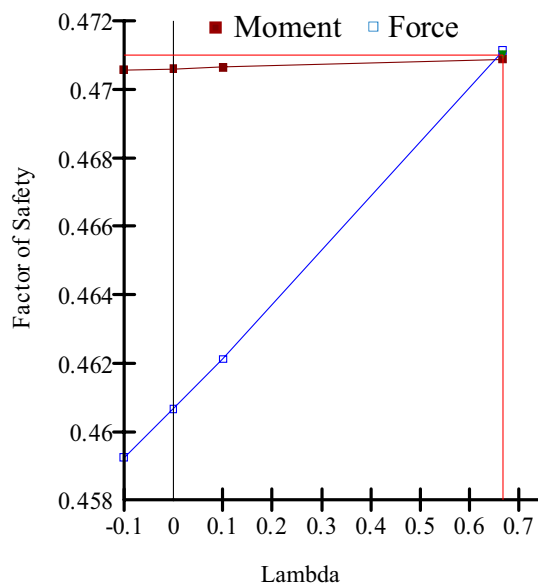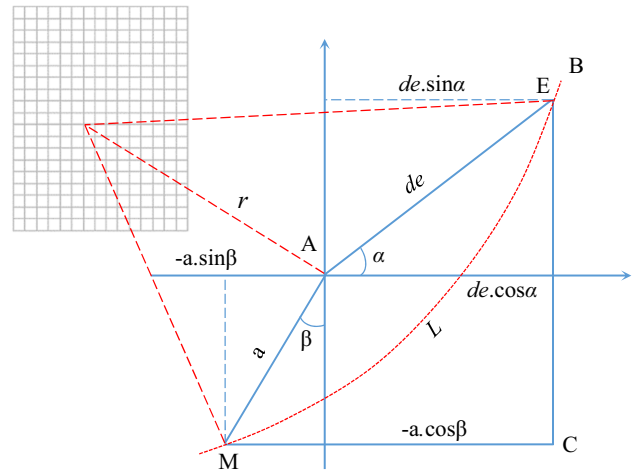

Fig. 5 Failure surface geometry

entry point E and exit point M. sliding surface entry and exit points are assumed in this particular research. From Fig. 2, x_{n+1} and x_1 are the x-coordinates of entrance and exit points on the slope face. The y-coordinates of a point on the sliding surface have entrance and exit points, which can be used to find out the length of failure arc. To solve this problem, it is assumed that the following Eq. 5 satisfied the failure circle formula. In Eq. 5, x_0, y_0 and r are unknown variables. To find these variables three equations are needed. Since, entry and exit points can satisfy the Eq. 5. Consequently, two of the equations created by inserting their coordinates in the Eq. 5 as:

$$(x - x_0)^2 + (y - y_0)^2 = r^2 \tag{5}$$

and the total length of sliding cure is given as:

$$L = \int_{xd}^{xk} \sqrt{(1 + (s'^2)}dx \tag{6}$$

$$s' = \frac{x - x_0}{\sqrt{r^2 - (x - x_0)^2}}. \tag{7}$$

From Eq. 6 L is length of failure arc which satisfy the Eqs. 8 and 9 as:

$$L = \int_{xd}^{xk} \frac{r}{\sqrt{r^2 - (x - x_0)^2}}dx \tag{8}$$

$$L = r\left(\sin^{-1}\frac{(de\,\cos\alpha - x_0)}{r} - \sin^{-1}\frac{(-\alpha\sin\beta - y_0)}{r}\right). \tag{9}$$

Fig. 4 Relationship between safety factor and lambda (λ)

The three equations, which are needed, can be evaluated with the help of Eq. 9 as follow:

$$\begin{cases} (de\cos a - x_0)^2 + (de\sin a - y_0)^2 = r^2 \\ (-a\cos\beta - x_0)^2 + (-a\sin\beta - y_0)^2 = r^2 \\ r\left(x\sin^{-1}\frac{de\cdot\cos\alpha - x_0}{r} - \sin^{-1}\frac{-a\sin\beta - y_0}{r}\right) = L \end{cases}.$$ (10)

The Eq. 10 can be solved by putting the value of geometric parameters (a, de, a, β, and L) and $a = h/\cos\beta$, and h is the height of slope and de is entry point distance. In Eq. 10, r is radius and $_0$, and $_0$ are the coordinates of slip circle. However, this geometric methodology is suitable for circular slip surface, where there are only three different control variables, so this method cannot be used to composite and non-circular slip surface. In addition, this method is not used material shear strength properties, thus there is no need to conduct laboratory test. Therefore, proposed geometrical method is simple and time saving as compare to other methods of slices.

3 Numerical simulation

3.1 Illustrative example

The promotion of China Pakistan Economic Corridor (CPEC) strategy has led to a large number of construction and exploitation in Pakistan. The stability of such large-scale engineering activities on hills or mountains along road side directly related to the progress of the project, economy and the safety of the workers [36]. Hence, the slope stability analyses are conducted by engineers to calculate the stability of road slopes, dam slopes, retaining wall and excavated slopes with critical sliding surface [35]. A loose rock cut slope is located along National Highway (N70) in Pakistan considered as a case study. The slope material is composed of boulder. Terrace is distributed in vast area of the project. It consists of 20-1000 mm
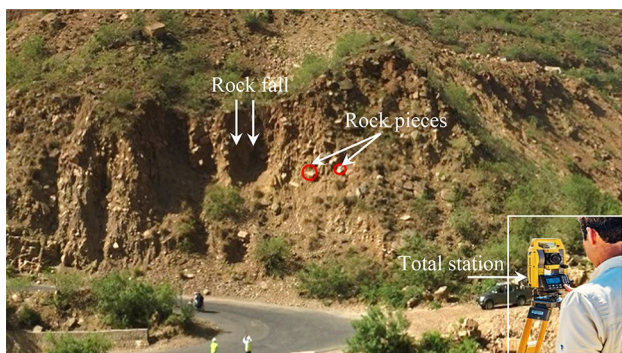
diameter of rounded rock pieces (Fig. 6). This formation is valley floor sediment and supposed to consist of two sandy layers. Water pressure measured with piezometer. The coordinates of water line are presented in Table 1.

3.2 Model parameters

The width and height of 70 m 35 m respectively, measured with total station (Fig. 6). Slope angle of 45° was recorded. The shear strength parameters of slope material assigned to corresponding region (Fig. 7a). Half-sin function and Mohr–Coulomb failure criterion is selected in current study. Trial slip surface entry and exit point are located as shown in Fig. 7a.

Stability factor and the location of the CFS are then simulated by SLOPE/W. An appropriate manner of realistically showing the result of the CFS is a safety map (Fig. 7b). All trial failure surfaces are shown with corresponding factor of safety. The location and distribution of all possible CFS

Table 1 Coordinates of piezometric line

Coordinates	X (m)	Y (m)
1	0	22
2	30	17
3	52	13
4	70	13

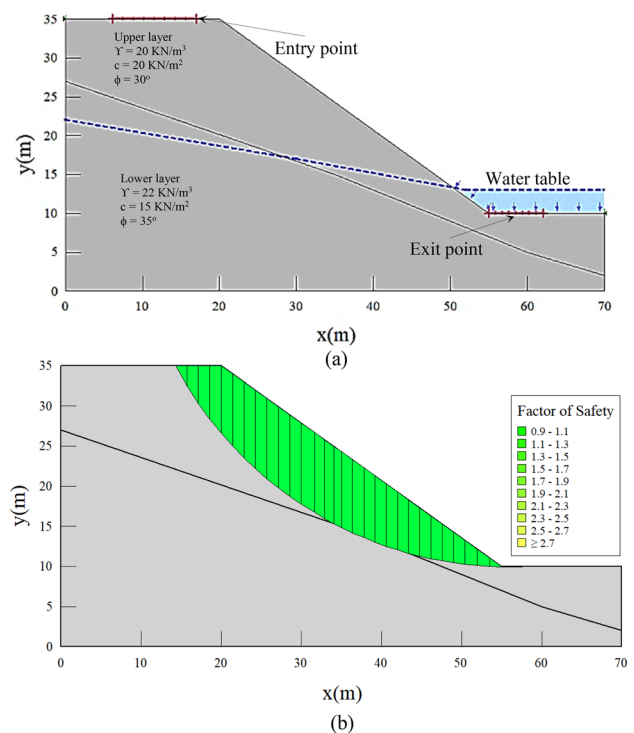Fig. 6 Topographical condition of loose rock slope and rock fall

Fig. 7 **a** Possible slope model **b** initial CFS from SLOPE/W analysis

can be seen in Fig. 7b. Figure 7b shows that critical failure surface initiate from crest and cut the slope near the toe.

3.3 Sliding mechanism for typical failure surfaces

In this sub-section the failure mechanism and the location of failure surfaces is analyzed at the various value of cohesion, friction angle and unit weight. Failure mechanism of a critical sliding surface could be analyzed from the deterministic examination and generating the different values of cohesion, friction and unit weight in the network of SLOPE/W computer code. The studied slope is heterogeneous and composed of two layers (upper layer and lower layer) of two different material. Three different cases are considered based on strength properties, namely, upper layer $c = 15$ (KN/m^2), $\phi = 20°$ and $\gamma = 18$ (KN/m^3); $c = 20$ (KN/m^2), $\phi = 25°$ and $\gamma = 19$ (KN/m^3) and $c = 25$ (KN/m^2), $\phi = 30°$ and $\gamma = 20$ (KN/m^3). Another is lower layer, $c = 10$ (KN/m^2), $\phi = 25°$ and $\gamma = 20$ (KN/m^3); $c = 15$ (KN/m^2), $\phi = 30°$ and $\gamma = 21$ (KN/m^3) and $c = 20$ (KN/m^2), $\phi = 35°$ and $\gamma = 22$ (KN/m^3). Sliding surface location and its sliding style for three sets of input parameters (c, ϕ, γ) are plotted in Fig. 8. The representative identifications according to Fig. 8 have many characteristics of CFSs location by varying the strength parameters. In Fig. 8, CFSs are located between the crest and the toe of loose rock slope and the sliding of the slope is a local failure at average value of strength parameters. The representative insights in Fig. 8 have different appearances of CFS failure mechanism and its location, which is categorized into three parts as follows:

(1) In first case, the CFS was shallow and cut the toe of slope as shown in Fig. 8a. The weak zone is comparatively small and is situated around the surface of the slope. The location of the CFS, in this case, is well dependable with the position of the weak zone and overall failure style is a local failure. Because the factor of safety (FS) for the CFS passing through the weak zone is smaller than that for other big CFSs representing an overall slope failure. When the failure of a slope surface happens in such a manner that the sliding surface cuts the slope surface or passes from slope toe, it is named slope failure as shown in Fig. 8a, b. In this case, the slip surface exit and entry points are respectively situated near the top and on the toe of slope surface.

(2) When the strength parameters were kept relatively large, the CFS was deep (Fig. 8b). In second case, the weak zones are relatively large and situated at the upper most portion of slope. The associated failure mechanism for a typical CFS is a narrow failure as shown in Fig. 8b. The observation for this particular case is that, the value of safety factor was lesser for
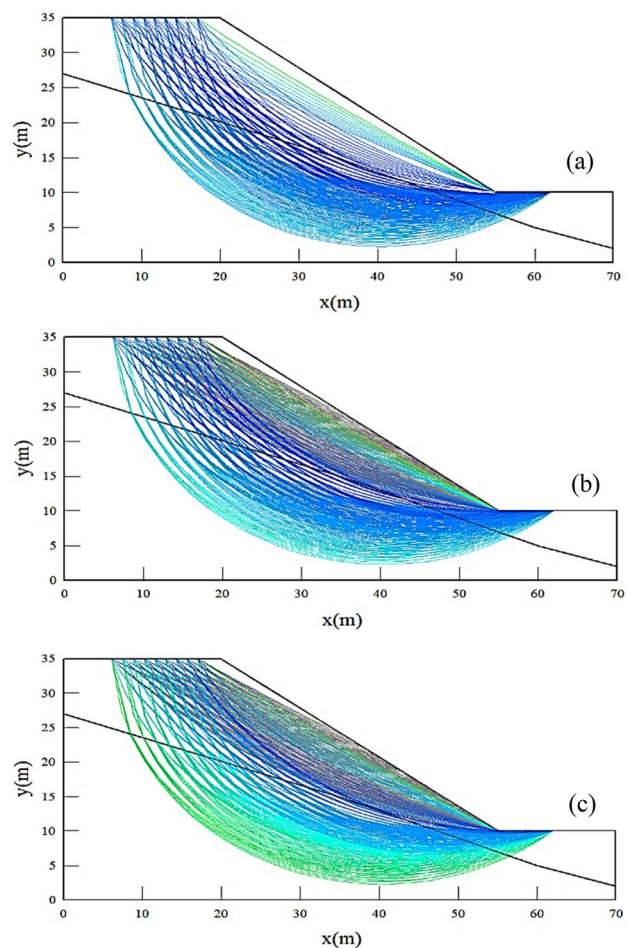

Fig. 8 Display of multiple trial slip surfaces **a** small value of strength parameters **b** comparatively large value of strength parameters **c** large value of strength parameters

big sliding surfaces and passing through the weak area of the slope that showing an overall circular failure.

(3) When the large value of strength parameters selected the CFS is located at the little distance from the toe and the slip mode of a loose rock slope is global slip (Fig. 8c). Because safety factor (FS) for a CFS is bigger as compared to other all-valid slip surfaces in the weak areas of slope. In this particular example, the loose rock slope sliding is a deep-seated failure and the position of CFS not dependable with the actual situation of the weaker areas. Because the weight of slope material is the part of the gravitational force and this is related to the size of the sliding body. The resistance shear force of slope material contains on two components, cohesion part and internal friction part. Apparently, as the volume of the sliding body decreased, the diminishing amount of related CFS was minor than that of sliding body. Especially, if the

input strength properties of slope kept constant and the volume of slippery body reduced, the weight of slope reduced more rapidly than the slope resistance. For a comparatively large CFS as displayed in Fig. 8c, the cohesion force is small enough to produce a safety factor for the weak area lesser than the safety factor for a global CFS.

It can be evidently seen from the above analysis, that the sliding characteristics for a heterogeneous loose rock slope (formed by colluvium material) with a moderately small value of strength parameters is a global slid in most cases. In certain cases, although potential slid may occur, but the related CFS have entry and exit points situated at the crest and near the toe of slope, respectively.

4 Discussion

In this section, the influence of cohesion force (c), internal friction (ϕ) and the depth of pore water pressure (PWP) on safety factor (FS), depth of failure surface (D), length of failure arc (L) and its distribution is discussed by using SLOPE/W software. The general failure surface with an exit or an entry points on the slope face are assigned to horizontal coordinates of lowermost and uppermost points of CFS. The distribution range of all valid slip surfaces show similar phenomena for this particular case.

4.1 Influence of cohesion

In this sub-section, the influence of cohesion (c) is analyzed for same slope model configuration. For this purpose, unit weight and angle of internal friction (ϕ) are chosen as 20 KN/m^2 and 30°, respectively. The value of cohesion (c) ranging from 10 KN/m^2 to 20 KN/m^2 is assigned in SLOPE/W software for analysis. Three different slope model are tested by varying the values of c as 10, 15 and 20 (KN/m^2), respectively. The summary of computed safety factors are graphically portrayed and all-valid failure surfaces fall in the limit of all possible trial slips. The distribution range of failure surfaces are consistent with safety map (Fig. 9). Cohesion force has a substantial effect on the safety factor of loose rock cut slope principally for larger values.

As clearly displayed in Fig. 9a–c, when the cohesion force is increased, than there are enormous gapes among the allocations of all valid failure surfaces. In addition, the FS and maximum D increased linearly (Fig. 9). The reason is that the cohesion is a strength parameter increasing this value increase in FS. In other words, very large or local slip surface are more likely to occur, as the cohesion is kept enormous.

As shown in Fig. 9a, b, there are no significant differences in-between FS and the allocations of failure surfaces when c = 10 and c = 20 (KN/m^2) for upper and lower layer, respectively. Hence, the cohesion is set to be 20 and 25 (KN/m^2) for upper and lower layer, respectively. In addition, all valid sliding surfaces are a band of curves with different sizes, shape and locations. Safety factor and the distribution range of all valid failure surfaces suddenly increased with an increasing cohesion parameter as shown in Fig. 9c. The normal value of c with any probable failure surface is near to the average value of cohesion and a possible CFS is likely to run across both layers of slope material as shown in Fig. 9b, c. Hence, when the safety factors are comparatively small than the affected area and the distribution range of failure surfaces were larger for large safety factors as compare to small safety factors. This mechanism could be also examine by comparing the all-valid slip surfaces in Figs. 9 and 10.

The spatial changeability effect of cohesion on maximum failure length (L) is also examine in this study. The failure arc was supposed to be initiated from the crest (entry point) and cut the slope from or near the toe (Fig. 9). Figure 9 also shows the effect of c on L. Changing the value of c also change in failure arc length and position (Fig. 9). When cohesion was 15, 20 and 25, (KN/m^2) to be set the maximum length of failure arc is 48.8 m, 50.2 m and 50.4 m recorded, respectively. Failure arc length evaluated by the equation system presented in Sect. 2.3 was 50.0 m, which is consistent the result determined from SLOPE/W software. It is clearly seen in Fig. 9 that by increasing the value of c L increased significantly.

4.2 Influence of friction angle

This sub-section mainly discussed the changeability influence of angle of internal friction (ϕ) on the FS, maximum D, L and distribution range of all valid failure surfaces. As compare to cohesion parameters the friction parameter usually has a smaller effect on FS, depth and the slip surface distribution (e.g., [37]). Same procedure as for cohesion is adopted to investigate the effect of internal friction. By varying the value of friction angle, for both layers, three cases were investigated through SLOPE/W. The values of friction angle are set to be 20°, 25°, 30° and 25°, 30° and 35° for upper layer and lower layer, respectively. The reason is that the value of ϕ is varying from 20° to 35° for studied case. Unit weight and cohesion are set to be 20 KN/m^3 and 15 KN/m^2, respectively. Figure 10a–c plot the value of D and the distributions range of all valid trial failure surfaces for slope considering different values of friction angle. As the value of ϕ increased, the FS and distribution range of failure surfaces also increased significantly, but decrease

Fig. 9 Display of multiple trial slip surfaces **a** small value of cohesion **b** comparatively large value of cohesion **c** large value of cohesion

(a)

(b)

(c)
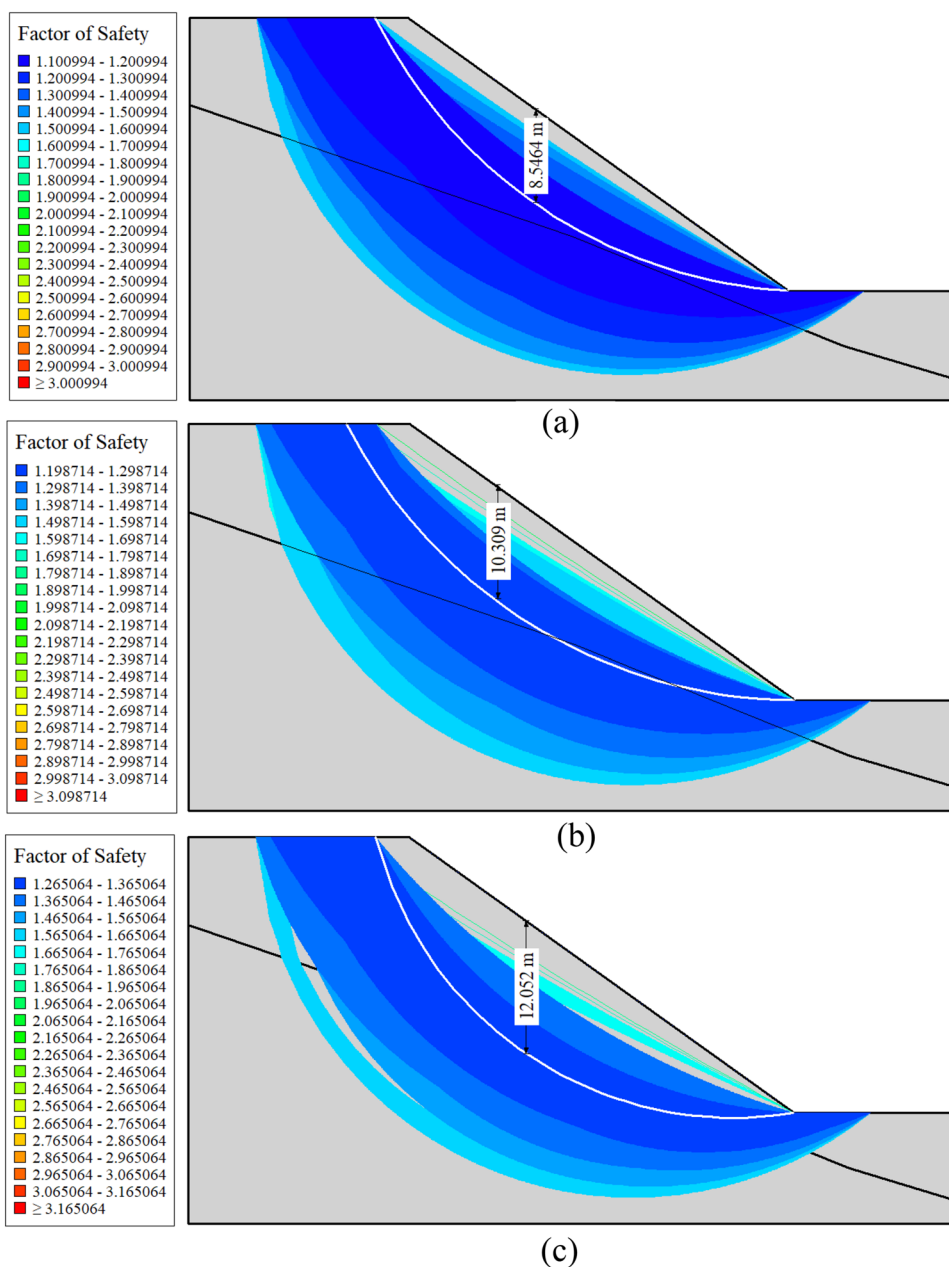
in the depth of slip surface (Fig. 10). Local failures happened in first two cases as $\phi = 20°$ and 25°, and 25° and 30° selected for both layers, respectively (Fig. 10a, b). When the value of ϕ is 30° and 35° chosen, no local failure occurs as shown in Fig. 10c. The reason is that ϕ is a strength parameter increasing this increase in material resistance force, which produced greater FS (Fig. 10c). In other words, when the value of ϕ is large, all trial failure surfaces are extremely likely to enter the slope from the crest (entry point) and cut the slope near the toe. By contrast, when the value of ϕ is comparatively small, local failures have an exit and entry points situated on the crest and around the toe of the loose rock slope.

There were no large variations among the distributions of sliding arcs as c and ϕ are modeled in software. The reason is that there are no clear weak zones were founded near the slope surface. In addition, the more representative CFS is deep in both cases (Fig. 10a, b). While, as friction increased the distribution range of possible failure surfaces also increased (Fig. 10c), and these insights agree well with the results published by Ahmed et al. [37]. Nevertheless, in case of friction angle CFS is not cross the lower layer of slope material as shown in Fig. 10. The reason is that, for angle of internal friction, the whole slope area is almost homogeneous. Figure 10 also shows the variability effect of internal friction (ϕ) on the L. The length of failure

Fig. 10 Display of multiple trial slip surfaces **a** small value of angle of internal friction **b** comparatively large value of angle of internal friction **c** large value of angle of internal friction

(a)

(b)

(c)
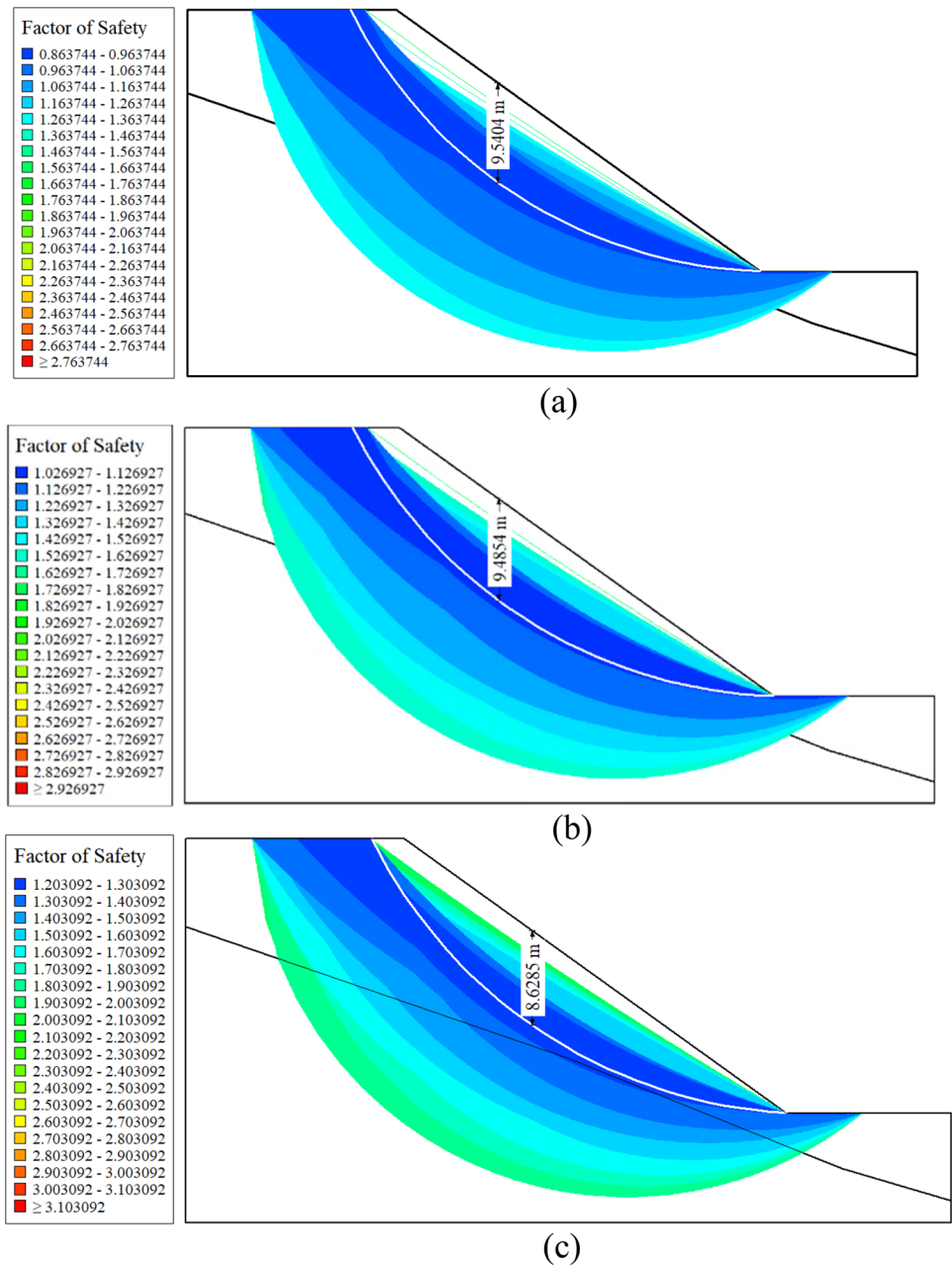
arc (*L*) changed from 58.33 m. 48.88 m and 47.62, when friction angles 25°, 30° and 35° were selected, respectively.

4.3 Influence of pore water pressure

The pore water pressure is one of the key factor affecting slope stability. When the whole slip surface cuts the water zone, and or some slices of the sliding mass lays within the water zone then this leads to sudden rise in the water pressure on the failure surface, which decreases the value of FS and also change the depth (*D*) of the possible sliding surface of the slope. The shape of CFS of the slope might be circular or spherical and might be shallow or deep-seated

depends on the pore water distribution and material profile in the slope [38].

In this sub-section, the effect of the depth of the water zone on the failure mode is also investigated choosing the minimum material strength properties for same slope model configuration. Figure 11 illustrates the locations of the potential CFSs when the depth of the water zone was 15 m, 20 m, and 25 m, respectively. The overall trend is that the CFS for composite type is deep than that of circular type (Fig. 11).

Two cases, based on material maximum and minimum shear strength properties (SSP), are considered to evaluate the different effects of pore water pressure on the
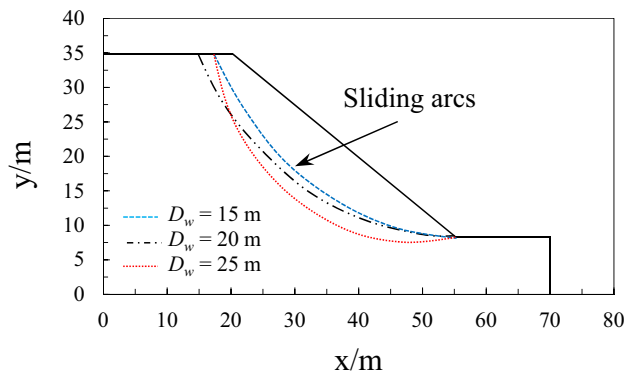
Fig. 11 Locations of the potential CFS when the depth of the water zone (D_w) is 15 m, 20 m and 25 m
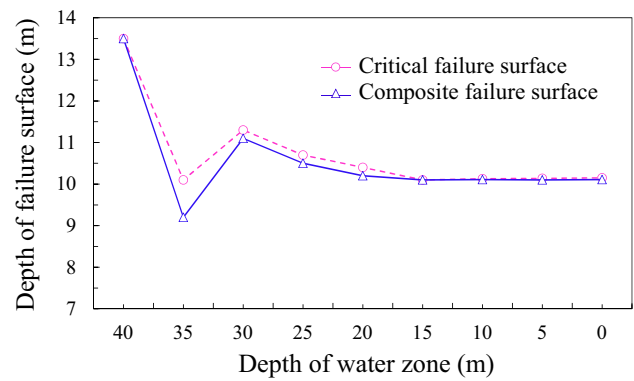

Fig. 13 Variation of the depth of the failure surface versus the depth of the water zone
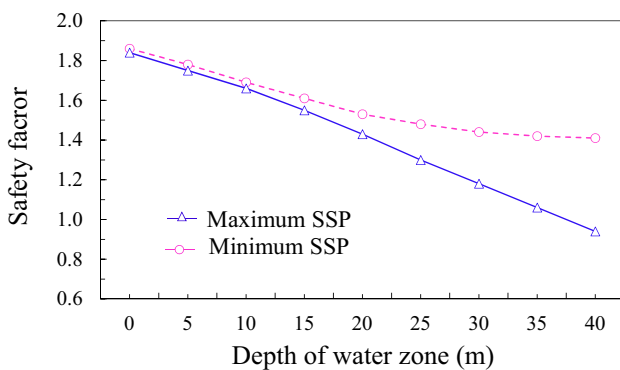

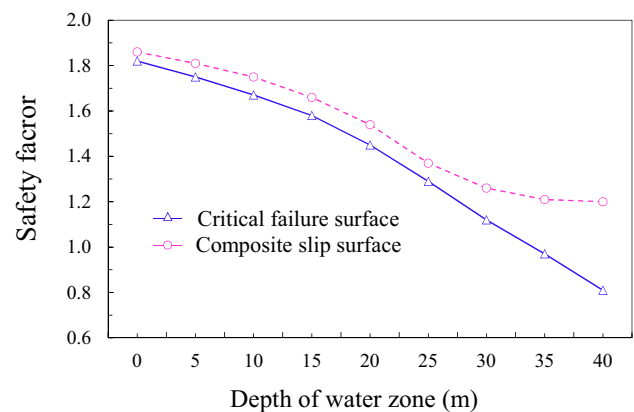**Fig. 12** Relationship between the safety factor and the depth of the water zone

Fig. 14 Safety factors of the slope under different failure modes

slope stability factor. The safety factors of the slope under both material properties are plotted versus the depth of the water zone in Fig. 12. FS of the loose rock slope, apart of the simulation technique, decreased by increasing the height of the water zone considering maximum and minimum material shear strength properties (Fig. 12). At both material strength properties, the safety factor of the cut slope showed a decreasing trend (linear) by increasing the height of the water zone. Which means that the increase in water zone depth plays a big role in altering the slope stability. The reason for this is that the slip surface is situated within the water zone and thus the variability effect of unit weight and other strength parameters are not much significant for the stability of the slope. At the material minimum strength parameters (SSP), the safety factor of the slope drops slowly (Fig. 12). As the depth of the water zone reached at 30 m, the FS maintain the value of 2.42 (Fig. 12). When the depth of the water zone was 1 m, the safety factor was almost consistent with first case (Fig. 12). The reason is that increasing the height of pore water increase in the weight of material, result in decrease

in FS. In addition, c and ϕ are resisting forces by reducing these decreases in FS. It can be concluded that by ignoring the pore water leads to the overestimate of the FS of the slope.

The effect of water zone height on the depth of the slope failure modes (critical or composite) investigated as shown in Fig. 13. The depth of both CFS and composite failure surface suddenly decreased first and then increased by increasing the depth of the water zone (Fig. 13). At maximum and minimum material properties, there is no big difference between the depths of CFS and composite failure surface. The reason is obvious and not repeated herein.

Figure 14 shows the relationship between safety factors (SF) of the slope and the depth of water zone under different failure modes e.g., circular or composite. In the Fig. 14, the safety factors corresponding to circular slip surface are consistently lower than those corresponding to composite slip surface, which is consistent with the observation in Fig. 12. This indicates that under the situation when water table exists, the slope is more exposed to landslide with composite slip surface.

The CFS is mostly to be affected by the mishmash of c and ϕ. It means that cohesion and friction parameters are resisting forces, decreasing these value leads to decrease in the value of FS, D, and de and slip surface distribution. Deep-seated or local failures may take place if the spatial (longitudinal) changeability of cohesion and friction is considered. This is worth observing that potential slope slips can take place in authenticity (e.g. [37],). This detail shows the significance of choosing the spatial change-ability influence of strength properties in slope stability analysis [39]. These results indicate that under the circumstances when pore water pressure exists, the loose slope is more exposed to slip with critical failure surface.

Therefore, it can be concluded that the effect of strength parameters for a loose rock material are helpful to choose appropriate value of these input parameters (i.e., cohesion and friction) for slope reinforcement design. Meanwhile, the factors of safety (FS) at $c = 20$ KN/m^2 and $\phi = 30°$ for CFS is obviously more than one. These values can be enhanced, based on the actual situation, using related rock reinforcement measures, such as anchor length.

4.4 Comparison of failure surface of slope by SLOPE/W and FLAC

In this sub-section, the SLOPE/W and FLAC^{3D} software was selected to compare the prediction of sliding surface of loose rock slope. The boundary and geometry conditions in FLAC^{3D} software were kept same as those in SLOPE/W software. The same material properties which are presented in Sect. 3.3 and other material constants were Poisson's ratio $\mu = 0.33$ and Young's modulus $E = 60$ MPa. FLAC^{3D} uses strength reduction technique to search possible value of safety factor (FS). In this method, c and ϕ are reduced with altered values of SRF until slope slip take place as:

$$C_f = c/f \tag{11}$$

$$\varphi_f = arctan\left(\frac{tan\varphi}{f}\right) \tag{12}$$

where c_f is reduced cohesion, φ_f reduced internal friction angle and f is safety factor. With increasing reduction factor the displacement also increases [40].

The safety factor FS = 0.86, 1.02 and 1.2 obtained via SLOPE/W (shown in Fig. 10) is consistent with FS = 0.88, 1.06 and 1.16 attained via FLAC^{3D} (Fig. 15). Regarding the prediction of the possible sliding mechanism of slope,

the distribution of the shear strain attained via FLAC^{3D} is presented in Fig. 15. This can be clearly observed from the chart that the shear strain localization band take place firstly followed by the development of the clear sliding surface of the loose rock slope. As can be observed form the Fig. 15, the numerical findings are same as far as the size and shape of the sliding surface of the studied slope is considered, however the positions are considerably different.
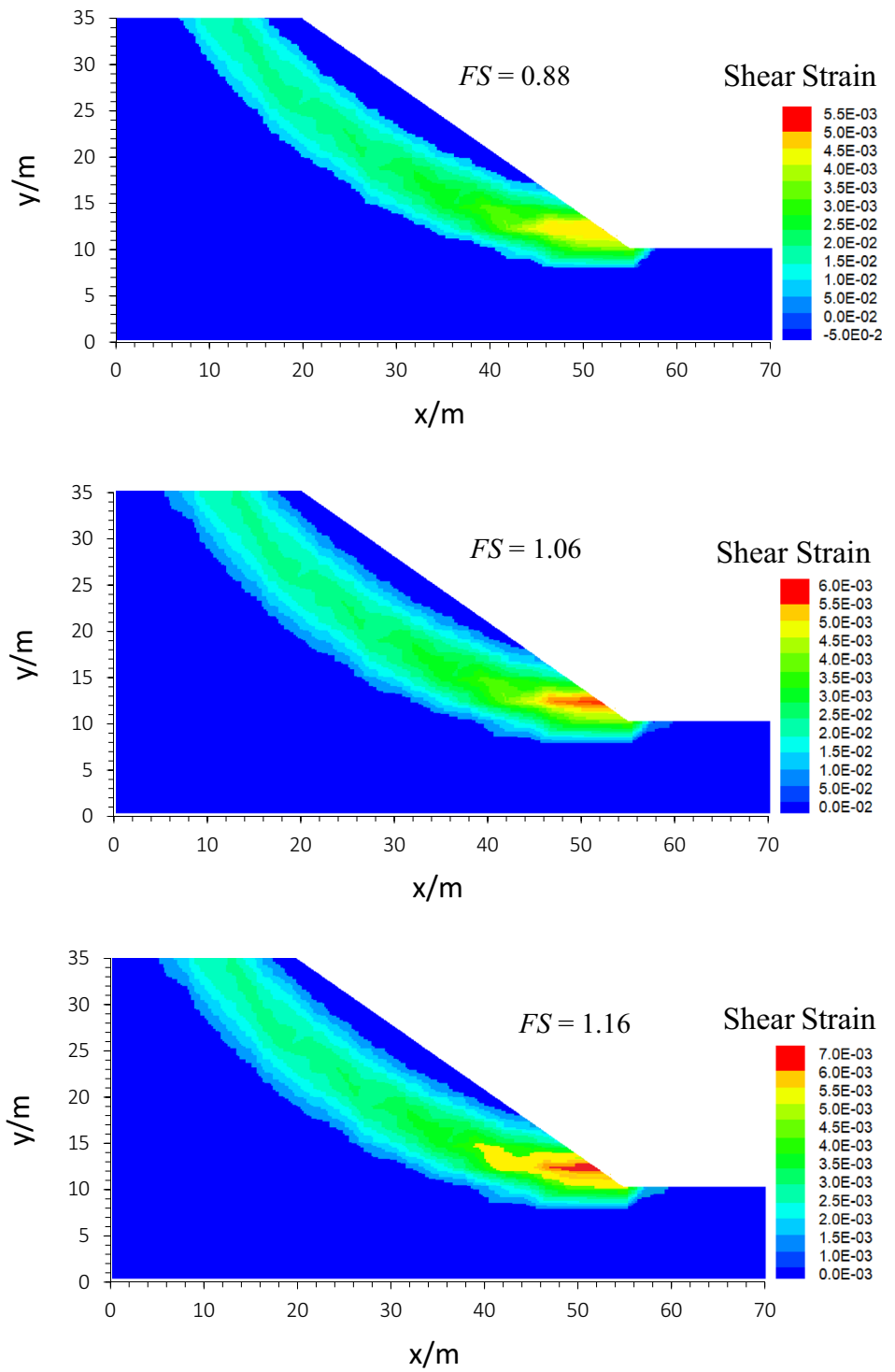
On the other hand, SLOPE/W has certain benefits over FLAC^{3D} with respect to material heterogeneity problems. It can be concluded that material heterogeneity problems can be captured practically well by the SLOPE/W software to avoid an extremely skewed mesh in FLAC^{3D}. For that reason, this recommends that SLOPE/W is more appropriate computer code to FLAC^{3D} when this comes to forecasting the sliding surface of heterogeneous material subjected to water zone.

5 Conclusions

In this study, a new search procedure based on the geometrical parameters is presented to estimate the length of failure arc. The failure mechanism of critical failure surface (CFS) and variability effect of strength parameters, and the depth of water zone on the distribution of CFS is examine by SLOPE/W software. The correctness of results is checked by FLAC^{3D} software. Results show that the rock slope formed by loose material can merely produce a global failure by ignoring the strength properties but with an increasing these properties the distribution range of CFSs increases. The pore water pressure (PWP) also plays a dominant role in altering the slope stability. Comparing the SFs and the locations of the failure surfaces, the landslides with composite slip surfaces are much easier to occur for loose rock slope subjected to water pressure.

The method is presented to estimate the length of sliding arc (L) provides the new researcher with a valuable superfluous procedure of analyzing loose rock slope stability. It is also noted that the current study underestimate the length of failure arc for loose rock slope due to the assumptions of sliding surface entry and exit points. The current geometrical method cannot estimate the value of FS, so this method should be modified in future research.

Fig. 15 The development of failure surface depicted by corresponding shear strain increment

Compliance with ethical standards

Conflict of interest On behalf of all authors, the corresponding author states that there is no conflict of interest.

References

1. Wang Y, Huang J, Tang H (2020) Automatic identification of critical slip surface of slopes. J Eng Geol 273:105672
2. Zhou X, Huang X, Zhao X (2020) Optimization of the critical slip surface of three-dimensional slope by using an improved genetic algorithm. J Eng Geol 20(8):04020120
3. Li L, Wang Y, Zhang L, Choi C, Ng C (2019) Evaluation of critical slip surface in limit equilibrium analysis of slope stability by smoothed particle hydrodynamics. Int J Geomech 19(5):04019032
4. Johari A, Mousavi S (2019) An analytical probabilistic analysis of slopes based on limit equilibrium methods. Bull Eng Geol Environ 78(6):4333–4347
5. Qi XH, Li DQ (2018) Effect of spatial variability of shear strength parameters on critical slip surfaces of slopes. J Eng Geol 239:41–49
6. Chen X, Zhang L, Chen L, Li X, Liu D (2019) Slope stability analysis based on the coupled Eulerian–Lagrangian finite element method. Bull Eng Geol Environ 78(6):4451–4463
7. Kalatehjari R, Ali N, Kholghifard M, Hajihassani M (2014) The effects of method of generating circular slip surfaces on determining the critical slip surface by particle swarm optimization. Arab J Geosci 7(4):1529–1539
8. Mishra M, Ramana GV, Maity DJ (2020) Multiverse optimisation algorithm for capturing the critical slip surface in slope stability analysis. Geotech Geol Eng 38(1):459–474
9. Wang J, Ji H (2013) Analysis of rock slope stability on the basis of limit equilibrium method. Adv Mater Res Trans Tech Publ 711:333–337
10. Liu S, Shao L, Li H (2015) Slope stability analysis using the limit equilibrium method and two finite element methods. Comput Geotech 63:291–298
11. Bishop AW (1955) The use of the slip circle in the stability analysis of slopes. Geotechnique 5(1):7–17
12. Baker R (1980) Determination of the critical slip surface in slope stability computations. Int J Numer Anal Methods Geomech 4(4):333–359
13. Jiang JC, Yamagami T (2004) Three-dimensional slope stability analysis using an extended Spencer method. Soils Found 44(4):127–135
14. Sun G, Cheng S, Jiang W, Zheng H (2016) A global procedure for stability analysis of slopes based on the Morgenstern-Price assumption and its applications. Comput Geotech 80:97–106
15. Baker R, Garber M (1978) Theoretical analysis of the stability of slopes. Geotchnique 28(4):395–411
16. Garber M (1973) Variational method for investigating the stability of slopes. Soil Mech Found Eng 10(1):77–79
17. Boutrup E, Lovell C (1980) Searching techniques in slope stability analysis. Eng Geol 16(1–2):51–61
18. Azarafza M, Asghari-Kaljahi E, Akgun H (2017) Numerical modeling of discontinuous rock slopes utilizing the 3DDGM (three-dimensional discontinuity geometrical modeling) method. Bull Eng Geol Environ 76(3):989–1007
19. Azarafza M, Akgun H, Ghazifard A, Asghari-Kaljahi E (2020) Key-block based analytical stability method for discontinuous rock slope subjected to toppling failure. Comput Geotech 124:103620
20. Azarafza M, Akgün H, Feizi-Derakhshi MR, Azarafza M, Rahnamarad J, Derakhshani R (2020) Discontinuous rock slope stability analysis under blocky structural sliding by fuzzy key-block analysis method. Heliyon 6(5):e03907
21. Zolfaghari AR, Heath AC, McCombie PF (2005) Simple genetic algorithm search for critical non-circular failure surface in slope stability analysis. Comput Geotech 32(3):139–152
22. Gao W (2016) Determination of the noncircular critical slip surface in slope stability analysis by meeting ant colony optimization. J Comput Civ Eng 30(2):06015001
23. Gordan B, Armaghani DJ, Hajihassani M, Monjezi M (2016) Prediction of seismic slope stability through combination of particle swarm optimization and neural network. Eng Comput 32(1):85–97
24. Cheng Y, Li L, Sc Chi, Wei W (2007) Particle swarm optimization algorithm for the location of the critical non-circular failure surface in two-dimensional slope stability analysis. Comput Geotech 34(2):92–103
25. Alemdag S, Kaya A, Karadag M, Gurocak Z, Bulut F (2015) Utilization of the limit equilibrium and finite element methods for the stability analysis of the slope debris: an example of the Kalebasi district (NE Turkey). J Afr Earth Sci 106:134–146
26. Morgenstern N, Price VE (1965) The analysis of the stability of general slip surfaces. Geotechnique 15(1):79–93
27. Spencer E (1967) A method of analysis of the stability of embankments assuming parallel inter-slice forces. Geotechnique 17(1):11–26
28. Cheng H, Zhou X (2015) A novel displacement-based rigorous limit equilibrium method for three-dimensional landslide stability analysis. Can Geotech J 52(12):2055–2066
29. Wang Y, Huang J, Tang H (2020) Global sensitivity analysis of the hydraulic parameters of the reservoir colluvial landslides in the Three Gorges Reservoir area, China. Landslides 17(2):483–494
30. Cheng Y (2003) Location of critical failure surface and some further studies on slope stability analysis. Comput Geotech 30(3):255–267
31. Cheng Y, Liu H, Wei W, Au S (2005) Location of critical three-dimensional non-spherical failure surface by NURBS functions and ellipsoid with applications to highway slopes. Comput Geotech 32(6):387–399

32. Wang S, Ahmed Z, Hashmi MZ, Pengyu W (2019) Cliff face rock slope stability analysis based on unmanned arial vehicle (UAV) photogrammetry. JG Geo-Energy Gf Geo-Resour 5(4):333–344

33. Hungr O, Salgado F, Byrne P (1989) Evaluation of a three-dimensional method of slope stability analysis. Can Geotech J 26(4):679–686

34. Malik MK, Karim IR (2020) Seepage and slope stability analysis of Haditha Dam using Geo-Studio Software. In: IOP conference series: materials science and engineering. IOP Publishing, p 022074

35. Fredlund D, Krahn J (1977) Comparison of slope stability methods of analysis. Can Geotech J 14(3):429–439

36. Azimi SR, Nikraz H, Yazdani-Chamzini A (2018) Landslide risk assessment by using a new combination model based on a fuzzy inference system method. KSCE J Civ Eng 22(11):4263–4271

37. Ahmed Z, Wang S, Jasim OH, Xu Y, Wang P (2020) Variability effect of strength and geometric parameters on the stability factor of failure surfaces of rock slope by numerical analysis. Arab J Geosci 13(21):1–12

38. Sun D, Li X, Feng P, Zang Y (2016) Stability analysis of unsaturated soil slope during rainfall infiltration using coupled liquid–gas–solid three-phase model. Water Sci Eng 9(3):183–194

39. Bai T, Hu X, Gu F (2019) Practice of searching a noncircular critical slip surface in a slope with soil variability. Int J Geomech 19(3):04018199

40. Nie Z, Zhang Z, Zheng H (2019) Slope stability analysis using convergent strength reduction method. Eng Anal Bound Elem 108:402–410

Publisher's Note Springer Nature remains neutral with regard to jurisdictional claims in published maps and institutional affiliations.